

2011

Femoral loading mechanics in the Virginia opossum (*Didelphis virginiana*): torsion and mediolateral bending in mammalian locomotion

W. Casey Gosnell

Michael T. Butcher

Takashi Maie

Richard W. Blob

Clemson University, rblob@clemson.edu

Follow this and additional works at: https://tigerprints.clemson.edu/bio_pubs

Recommended Citation

Please use publisher's recommended citation.

This Article is brought to you for free and open access by the Biological Sciences at TigerPrints. It has been accepted for inclusion in Publications by an authorized administrator of TigerPrints. For more information, please contact kokeefe@clemson.edu.

RESEARCH ARTICLE

Femoral loading mechanics in the Virginia opossum, *Didelphis virginiana*: torsion and mediolateral bending in mammalian locomotion

W. Casey Gosnell¹, Michael T. Butcher², Takashi Maie¹ and Richard W. Blob^{1,*}

¹Department of Biological Sciences, Clemson University, Clemson, SC 29634, USA and ²Department of Biological Sciences, Youngstown State University, Youngstown, OH 44555, USA

*Author for correspondence (rblob@clemson.edu)

Accepted 26 July 2011

SUMMARY

Studies of limb bone loading in terrestrial mammals have typically found anteroposterior bending to be the primary loading regime, with torsion contributing minimally. However, previous studies have focused on large, cursorial eutherian species in which the limbs are held essentially upright. Recent *in vivo* strain data from the Virginia opossum (*Didelphis virginiana*), a marsupial that uses a crouched rather than an upright limb posture, have indicated that its femur experiences appreciable torsion during locomotion as well as strong mediolateral bending. The elevated femoral torsion and strong mediolateral bending observed in *D. virginiana* might result from external forces such as a medial inclination of the ground reaction force (GRF), internal forces deriving from a crouched limb posture, or a combination of these factors. To evaluate the mechanism underlying the loading regime of opossum femora, we filmed *D. virginiana* running over a force platform, allowing us to measure the magnitude of the GRF and its three-dimensional orientation relative to the limb, facilitating estimates of limb bone stresses. This three-dimensional analysis also allows evaluations of muscular forces, particularly those of hip adductor muscles, in the appropriate anatomical plane to a greater degree than previous two-dimensional analyses. At peak GRF and stress magnitudes, the GRF is oriented nearly vertically, inducing a strong abductor moment at the hip that is countered by adductor muscles on the medial aspect of the femur that place this surface in compression and induce mediolateral bending, corroborating and explaining loading patterns that were identified in strain analyses. The crouched orientation of the femur during stance in opossums also contributes to levels of femoral torsion as high as those seen in many reptilian taxa. Femoral safety factors were as high as those of non-avian reptiles and greater than those of upright, cursorial mammals, primarily because the load magnitudes experienced by opossums are lower than those of most mammals. Thus, the evolutionary transition from crouched to upright posture in mammalian ancestors may have been accompanied by an increase in limb bone load magnitudes.

Key words: locomotion, biomechanics, bone stress, opossum, safety factor.

INTRODUCTION

For most tetrapod vertebrates, limb bones play a crucial role in the support of the body and transmission of muscular and propulsive forces. The forces to which limb bones are exposed during terrestrial locomotion likely impose some of the highest loads that these structures experience (Biewener, 1990; Biewener, 1993). However, a growing body of data now indicates that substantial differences in loading mechanics (both loading regimes and magnitudes) are present among tetrapod lineages with different characteristic locomotor patterns. For example, early studies of mammals running with upright, parasagittal limb postures indicated that anteroposterior (AP) bending was generally the most important loading regime, and that the ratio of limb bone strength to load magnitude (i.e. safety factor) was generally between two and four (Rubin and Lanyon, 1982; Biewener et al., 1983; Biewener et al., 1988). In contrast, more recent data from amphibians and reptiles that use sprawling limb posture indicated prominent limb bone torsion in addition to bending, with limb bone safety factors of usually at least five and sometimes exceeding 10 (Blob and Biewener, 1999; Blob and Biewener, 2001; Butcher and Blob, 2008; Butcher et al., 2008; Sheffield and Blob, 2011; Sheffield et al., 2011). Yet, a view that such patterns have strict phylogenetic associations may not be

appropriate. For example, significant torsional loading has been described for the hindlimb elements of running birds (Carrano, 1998; Main and Biewener, 2007) and laboratory rats (Keller and Spengler, 1989), species that move the limbs in essentially parasagittal planes, but hold the femur in a more crouched position than the upright stance typical of the cursorial mammals (e.g. horses and dogs) examined in most early studies (Rubin and Lanyon, 1982; Biewener et al., 1983). Limb posture, therefore, also appears to play a crucial role in the mechanics of limb bone loading.

To evaluate how limb bone loading patterns have diversified across clades that use different characteristic postures and locomotor kinematics, we recently analyzed *in vivo* strains from the femora of the Virginia opossum, *Didelphis virginiana* (Kerr 1792), during running on a treadmill (Butcher et al., 2011). Examination of this species has expanded perspectives on the diversity of limb bone loading mechanics in several ways. First, as a running marsupial, opossums belong to a lineage that is phylogenetically intermediate between the mammals and reptiles that have received previous study (Meyer and Zardoya, 2003), and could provide insight into transitions in loading patterns between these groups. Second, opossums provide additional limb bone loading data from a mammalian species that uses a more crouched limb posture (Jenkins,

1971), testing whether patterns observed in rats might hold more generally. Our strain measurements gave estimates of femoral safety factors moderately higher than those evaluated for other mammalian lineages, and also indicated significant femoral torsion in opossums in addition to bending (Butcher et al., 2011). Moreover, planar strain analyses indicated a general mediolateral (ML) orientation to femoral bending (Butcher et al., 2011). This result was surprising, considering that the opossums were running with essentially fore–aft oscillations of the limbs, and previous force platform data from small mammals (chipmunks and ground squirrels) had indicated AP bending of the femur in those species (Biewener, 1983).

Although *in vivo* strain data provide crucial information on the distribution of loads for specific locations on bone surfaces, they are often insufficient to indicate the mechanisms underlying the generation of the loads that are measured. To provide a complementary assessment and help evaluate the mechanisms contributing to the loading patterns of opossum femora, we evaluated the stresses developed in the femur of *D. virginiana* by collecting synchronized, three-dimensional kinematic and force platform data from this species during terrestrial locomotion. By integrating data on limb position with data on locomotor ground reaction forces (GRFs), analyses of joint equilibrium can be performed to clarify both the external and muscular forces and moments acting on limb bones (Biewener and Full, 1992). Although the estimates of load magnitude that these analyses generate are indirect, significant insights into the mechanics underlying bone loading patterns can be produced (Blob and Biewener, 2001). The use of three-dimensional analyses could be particularly helpful in this regard, as most previous force-platform-based analyses of mammalian limb bone loading have used two-dimensional measurements of kinematics and GRF (e.g. Alexander, 1974; Biewener, 1983; Biewener et al., 1988), with which observations of torsion and ML bending would be difficult. Thus, this study will provide insight into both the specific factors contributing to the loads experienced by opossum limbs and, more generally, the sequence of changes in limb bone loading mechanics through the evolutionary diversification of tetrapods.

MATERIALS AND METHODS

Animals

Force-platform data were collected from four Virginia opossums, *D. virginiana* (three females and one male, 1.6–3.9 kg body mass). Opossums were collected using live traps (Havahart EasySet, 0.8 × 0.3 × 0.4 m; Forestry Suppliers, Jackson, MS, USA) in Pickens, Anderson and Greenville Counties, SC, USA. Opossums were housed at room temperature (20–23°C) in medium-sized primate enclosures (~1 × 1 × 0.75 m) containing a litter pan and a pet carrier to provide cover for the animals. Opossums were exposed to 12 h:12 h light:dark cycles, provided with water, and fed with commercial cat food daily. Prior to experiments, fur was shaved from the lateral aspect of the right hindlimb of each opossum, and anatomical landmarks of interest were located by palpation and marked on the skin using dots of black marker surrounded by white correction fluid. Guidelines and protocols approved by the Clemson University IACUC (AUP ARC2007-030 and 2009-059) were followed during all procedures. At the conclusion of force-platform trials and complementary measurements of *in vivo* bone strain (Butcher et al., 2011), opossums were anesthetized (20 mg kg⁻¹ i.m. ketamine injection) and then killed by an overdose of pentobarbital sodium solution (Euthasol®, Delmarva Laboratories Inc., Midlothian, VA, USA; 200 mg kg⁻¹ intracardiac injection). Experimental specimens were then frozen for later dissection and measurement of anatomical variables.

Collection of kinematic and GRF data

Lateral and posterior views of opossums running with a trotting gait were filmed using a pair of digitally synchronized high-speed video cameras (Phantom v.4.1, Vision Research Inc., Wayne, NJ, USA) at 200 Hz. Successful trials consisted of the right hindlimb of an individual striking a custom-built force platform (K&N Scientific, Guilford, VT, USA) that was inserted into a wooden trackway [for details see Butcher and Blob (Butcher and Blob, 2008)]. The functional surface of the plate was restricted to an 11 × 10 cm area to increase the probability of recording isolated footfalls from a single limb. The surface of the platform was flush with the trackway, and the track and platform were coated with spray-grit and thin rubber, respectively, to reduce foot slippage.

Opossums were allowed to run at a self-selected speed during trials, and were encouraged by providing a shelter at the far end of the trackway and using a variety of stimuli, including gently squeezing the base of the tail and rubbing sandpaper or laboratory instruments together to create rasping noises. The trackway was kept at room temperature (20–23°C) and each individual was allowed several minutes of rest between trials, with extended rest periods when a specific stimulus no longer elicited a response. Trials judged suitable for analysis showed minimal overlapping contact of the right forelimb and hindlimb on the platform.

Highlighted anatomical landmarks (hip, knee, ankle, metatarsophalangeal joint, tip of digit four, and two points dorsal to the hip marking the anterior and posterior pelvic margins) were digitized from every frame of both lateral and posterior AVI video files using DLDataViewer2 software (Hedrick, 2008). Skin movement over landmarks appeared minimal, but may have contributed to some error in the location of joints during digitizing. Three-dimensional limb kinematics were calculated using custom MATLAB (v.7.9.0; The MathWorks Inc., Natick, MA, USA) routines that calibrated the two camera views, corrected for parallax, and allowed smoothing and normalization of traces from all trials to the same duration (101 points) by fitting quintic splines to coordinate data (Walker, 1998). Instantaneous animal speed throughout each trial was also calculated by differentiating the cumulative displacement of the posterior pelvic landmark.

The force platform resolved vertical, AP and ML components of the GRF. Specifications for the platform and data acquisition system were described in a previous paper (Butcher and Blob, 2008). Force data were collected at 5000 Hz using a custom LabVIEW (v.6.1; National Instruments, Austin, TX, USA) routine, with amplifier gains adjusted as appropriate to maximize platform sensitivity for each animal. The platform was calibrated daily in all three directions, and cross talk was negligible between force channels. The natural unloaded frequencies of each force plate component were 190 Hz, a value large enough compared with the stride frequency of opossums to limit confounding of the GRF signal.

Force and kinematic data were synchronized using a trigger that, when activated, simultaneously produced a 1.5 V signal in the force trace and flashed an LED visible in the video. All three components of the GRF measured while the right hindfoot contacted the platform were smoothed and normalized to 101 points using a quintic spline algorithm (Walker, 1998) in custom MATLAB routines, matching the number of points calculated for kinematic data. For consistency with our previous force-platform studies of sprawling species (Blob and Biewener, 2001; Butcher and Blob, 2008; Sheffield and Blob, 2011; Sheffield et al., 2011), the GRF point of application was initially calculated at the center of the portion of the foot in contact with the ground, and recalculated for each frame as the posterior portion of the foot was lifted from the ground during stance phase

(Carrier et al., 1994). The small size of opossum feet should limit any error incurred through this approach.

A custom MATLAB program was used to process synchronized video and force data to calculate the GRF magnitude, orientation and moments about each hindlimb joint, producing the input for analyses of femoral stresses. Moments about the hindlimb joints induced by gravity and the momentum of the limb were assumed to be negligible in our models because they are typically small relative to the moments produced by the GRF during stance, particularly for taxa in which the limbs are short and small in mass relative to the body (Alexander, 1974; Biewener, 1983; Biewener and Full, 1992).

Model of hindlimb muscle activity and bone stress analyses

Following the approaches of our previous analyses of GRFs in sprawling taxa (Blob and Biewener, 2001; Butcher and Blob, 2008; Sheffield and Blob, 2011; Sheffield et al., 2011), the forces acting on the hindlimbs of opossums were resolved into an anatomical frame of reference determined by the primary planes of motion of the limb segments. However, because opossums use limb motions that are much closer to parasagittal than horizontal (Jenkins, 1971), conventions for these planes differ from those for sprawling taxa: the ML plane contains both the femoral and tibial long axes, the AP plane contains the femoral long axis but is oriented perpendicular to the ML plane, and the dorsoventral (DV) plane is mutually perpendicular to the ML and AP planes. Using these conventions, extension of the knee joint occurs in the anterior direction with flexion in the posterior direction, whereas femoral adduction would occur in the medial direction and abduction in the lateral direction.

Femoral stress calculations similarly followed approaches established in our previous analyses of sprawling taxa (Blob and Biewener, 2001; Butcher and Blob, 2008; Sheffield and Blob, 2011; Sheffield et al., 2011). Stresses were calculated at mid-shaft, where bending moments are the greatest (Biewener and Taylor, 1986), and were imposed due to the action of both the GRF and muscular forces. To estimate muscle forces, limb joints were assumed to be in static rotational equilibrium; in addition, a further initial assumption was made that only muscles that would counteract the rotational moment of the GRF would be active (Alexander, 1974; Biewener, 1983; Biewener and Full, 1992). Yet, although all muscles that cross a joint and are active during stance could contribute to moments that would counter the moment imposed on a joint by the GRF, only forces exerted by muscles spanning the mid-shaft of the femur (Fig. 1, Table 1) contribute directly to calculations of peak bending stress (Alexander, 1974; Biewener et al., 1983; Blob and Biewener, 2001; Butcher and Blob, 2008). With these assumptions, the total muscle force (F_m) required to maintain equilibrium at a joint is calculated as:

$$F_m = R_{\text{GRF}} \times \text{GRF} / r_m, \quad (1)$$

where R_{GRF} is the moment arm of the GRF about the joint (calculated in custom MATLAB routines) and r_m is the moment arm of the muscles acting to oppose the moment of the GRF. If F_m was produced by the action of multiple muscles with different values of r_m , a weighted mean r_m was calculated for the group based on the physiological cross-sectional areas (PCSA) of each muscle, which are assumed to be proportional to the forces they exert (Alexander, 1974; Biewener and Full, 1992). Muscle moment arms were measured with digital calipers during specimen dissections with the right hindlimb held in midstance position, and PCSAs were calculated following published protocols (Biewener and Full, 1992).

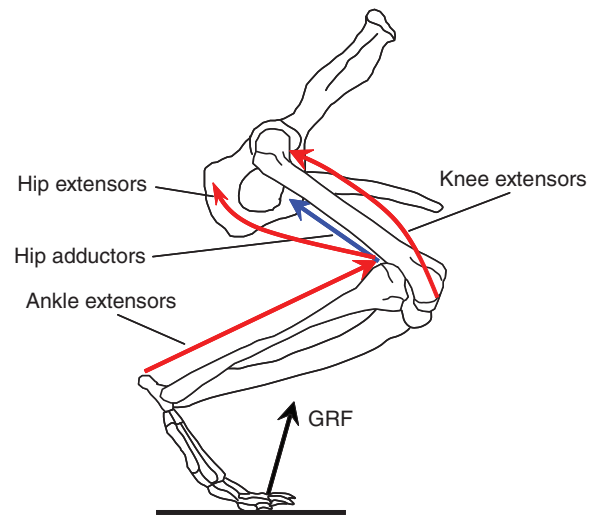


Fig. 1. Outline sketch (right lateral view) of the hindlimb skeleton of *Didelphis virginiana* illustrating the lines of action of the major muscle groups contributing to stresses in the femur during the stance phase of terrestrial locomotion for the anteroposterior (red arrows) and mediolateral (blue arrow) directions. These forces are elicited in response to the ground reaction force (GRF; black arrow). Sketch modified from Kemp (Kemp, 1982).

To evaluate the contributions of muscular forces to femoral stress, we constructed a model of muscle activity in the opossum hindlimb that included extensors of the ankle, flexors and extensors of the knee, and adductors and extensors of the hip (Fig. 1). Consideration of all of these muscle groups was necessary to evaluate the contributions of biarticular ankle extensors to total moments at the knee joint that might elevate the forces exerted by muscles spanning the femur (Alexander, 1974; Biewener, 1983; Schoenfuss et al., 2010). Because published data on hindlimb muscle activity were unavailable for opossums, our assessments of which muscles to consider followed the precedent of previous force-platform-based analyses of bone loading in small mammals (Biewener, 1983) and drew from available electromyographic (EMG) data for rats and cats (Rasmussen et al., 1978; Sullivan and Armstrong, 1978; Gruner and Altman, 1980; Roy et al., 1991; Gillis and Biewener, 2001; Thota et al., 2005) to supplement anatomical assessments of function specific for opossums (Romer, 1922).

Our model included the following key features. First, as in previous studies (Biewener, 1983; Blob and Biewener, 2001; Butcher and Blob, 2008; Sheffield and Blob, 2011; Sheffield et al., 2011), muscles are assumed to act in the same anatomical plane throughout stance phase. Second, at the ankle, our model focused on ankle extensors (i.e. foot plantarflexors) because the GRF exerts a flexor moment at the ankle for most of stance (see Results). Seven muscles contribute to ankle extension, of which four only oppose the GRF moment at the ankle (flexor digitorum longus, flexor hallucis longus, soleus and peroneus), but three are biarticular and also contribute to a flexor moment at the knee (gastrocnemius lateralis, gastrocnemius medialis and plantaris). Third, seven muscles (or muscle groups) contribute to extensor moments at the hip, but five (gluteal complex, caudofemoralis, crurococcygeus, obturator internus and obturator externus) insert proximally and were modeled as only contributing to hip moments, whereas the remaining two (biceps femoris and semitendinosus) span the length of the femur (Fig. 1) and also contribute to midshaft femoral bending stresses, placing the posterior surface in compression. Fourth, knee extensors

Table 1. Anatomical data from hindlimb muscles of experimental animals (*Didelphis virginiana*)

Muscle	op04			op05			op06			op07		
	A	θ	r_m									
Ankle extension												
Flexor digitorum longus	9.7	0	3.1	22.7	0	6.5	29.0	0	7.7	12.4	0	3.2
Flexor hallucis longus	6.4	0	3.1	19.0	0	4.3	83.2	0	7.3	24.3	0	2.6
Soleus	48.8	0	5.5	73.2	0	6.0	192.6	0	8.1	101.9	0	3.2
Peroneus	40.4	0	2.4	56.2	0	2.1	217.7	0	2.5	115.2	0	1.7
Gastrocnemius lateralis	43.2	0	6.9	110.7	0	6.6	37.1	0	7.7	130.8	0	7.9
			4.6 ^k			6.2 ^k			13.5 ^k			6.1 ^k
Gastrocnemius medialis	19.4	0	8.2	47.5	0	11.0	132.2	0	11.6	37.4	0	8.1
			4.9 ^k			9.6 ^k			14.6 ^k			6.8 ^k
Plantaris	10.3	0	6.9	20.9	0	5.4	97.1	0	10.2	30.8	0	7.9
			4.0 ^k			7.8 ^k			18.9 ^k			6.1 ^k
Knee extension												
Rectus femoris	68.6	5	3.8	105.9	5	9.0	279.0	5	12.2	217.9	5	4.8
Vastus medialis	38.4	0	4.6	75.2	0	9.3	140.0	0	10.2	147.5	0	4.5
Vastus intermedius	41.9	0	3.2	40.8	0	4.5	170.3	0	10.2	140.4	0	5.9
Vastus lateralis	36.4	0	4.6	108.1	0	5.3	245.8	0	9.1	52.9	0	6.0
Hip retraction												
Gluteal complex	139.1	0	2.9	134.8	0	3.8	248.7	0	7.7	275.3	0	5.1
Caudofemoralis	19.8	0	8.7	38.7	0	14.1	44.1	0	18.9	33.7	0	12.2
Crurcoccygeus	6.4	22	20.4	18.4	21	23.9	21.3	24	39.1	14.1	10	24.5
			27.1 ^k			30.9 ^k			37.6 ^k			24.9 ^k
Obturator internus	15.6	0	7.7	18.8	0	5.6	22.9	0	6.0	25.4	0	11.5
Obturator externus	41.5	0	3.7	83.8	0	7.0	98.2	0	9.3	73.1	0	2.9
Biceps femoris	43.1	15	15.7	88.2	18	21.4	90.6	15	16.1	96.4	8	6.2
			15.2 ^k			16.0 ^k			15.2 ^k			18.8 ^k
Semitendinosus	21.3	22	15.9	38.8	20	28.4	51.8	18	18.8	38.4	16	9.5
			26.8 ^k			18.7 ^k			18.3 ^k			17.4 ^k
Hip adduction												
Adductor magnus	49.7	5	11.4	97.0	20	29.7	131.6	20	11.1	37.3	15	15.3
Adductor longus	36.3	10	15.7	189.6	15	21.4	84.9	20	16.1	104.8	5	6.2
Adductor brevis	20.2	20	13.4	73.5	10	10.0	35.2	17	16.7	127.8	20	14.4
Gracilis	33.2	20	20.4	21.6	17	23.9	81.8	18	39.1	75.1	15	24.5
			17.7 ^k			16.8 ^k			29.6 ^k			24.5 ^k
Semimembranosus	46.4	20	23.4	41.5	20	26.0	108.6	19	26.6	55.2	15	15.3
			14.9 ^k			15.9 ^k			12.0 ^k			11.3 ^k

A, physiological cross-sectional area of muscle (mm²); θ , angle between the muscle and the long axis of the femur (deg); r_m , moment arm of the muscle (mm) about the joint (a superscripted k indicates knee flexion).

(rectus femoris and the vasti) spanning the anterior surface of the femur counter the combined knee flexor moments of the GRF and ankle extensors that span the knee. The bending moment induced by the knee extensors opposes that induced by hip extensors, placing the anterior femoral cortex in compression. And fifth, five hip adductor muscles (adductor magnus, adductor longus, adductor brevis, gracilis and semimembranosus) counter the abductor moment of the GRF at the hip (see Results), with all five spanning the midshaft. In a significant revision of previous models of bone loading in small mammals based on force-platform analyses (Biewener, 1983), our three dimensional measurements of GRF moments allow the action of these muscles to be aligned with their anatomical position, rather than grouped with hip extensors. Thus, contraction of these muscles can be modeled as bending the femur to place its medial surface in compression.

Using the model outlined, muscle force calculations were made for each of the 101 time increments for each trial using custom MATLAB routines. Complications with calculating muscular contributions to femoral torsion (i.e. shear stresses) led us to desist from making such estimates (Blob and Biewener, 2001; Butcher and Blob, 2008; Sheffield and Blob, 2011). Nonetheless, the model we apply in this study accounts for known co-activation of antagonist

muscle groups to the extent possible, and allows us to calculate estimates of muscle forces comparable to those from previous analyses (Biewener, 1983; Blob and Biewener, 2001; Butcher and Blob, 2008).

After calculating estimates of muscle forces, bending moments along with axial and bending stresses were calculated following published methods (Biewener, 1983; Biewener and Full, 1992; Beer and Johnston, 1997) modified for three-dimensional analysis (Blob and Biewener, 2001; Butcher and Blob, 2008; Sheffield and Blob, 2011). Linear and angular anatomical variables (Table 2) were measured from digital photographs of the femur of each opossum. Cross-sectional anatomical variables (cross-sectional area, second moments of area and polar moment of area; Table 2) were calculated from digital photographs of mid-shaft sections cut from each bone, traced in Microsoft PowerPoint and input into custom software (Lieberman et al., 2003). Bending moments and stresses were calculated for perpendicular ML and AP directions (Blob and Biewener, 2001), and accounted for bending induced by axial forces due to the moment arm of bone curvature, r_c (Biewener, 1983). Net bending stress magnitude at the mid-shaft of the femur was calculated as the vector sum of bending stresses in the AP ($\sigma_{b/AP}$) and ML ($\sigma_{b/ML}$) directions (Blob and Biewener, 2001; Butcher and

Table 2. Anatomical data from femora of experimental animals (*D. virginiana*)

Measurement	op04	op05	op06	op07
Length (mm)	65.87	79.68	83.84	84.95
A (mm ²)	11.01	20.68	35.20	24.73
r _{c(ML)} (mm)	-5.97	-5.57	-8.10	-6.31
r _{c(AP)} (mm)	-1.30	0.45	0.67	0.57
y _{ML} (mm)	2.23	3.80	3.74	3.18
y _{AP} (mm)	2.04	4.16	3.65	3.27
I _{ML} (mm ⁴)	17.70	52.60	157.00	79.70
I _{AP} (mm ⁴)	20.40	62.50	164.00	86.20
J (mm ⁴)	38.10	115.10	321.00	165.90

In subscript notations, AP denotes the anatomical anteroposterior direction for the femur and ML denotes the anatomical mediolateral direction for the femur. A, cross-sectional area of bone; I, second moment of area; J, polar moment of area; r_c, moment arm due to bone curvature; y, distance from neutral axis to cortex.

Curvature sign conventions for ML: positive, concave lateral; negative, concave medial; curvature sign conventions for AP: positive, concave posterior; negative, concave anterior.

Blob, 2008; Sheffield and Blob, 2011), allowing the orientation of peak bending stress to be calculated as:

$$\alpha_{b/net} = \tan^{-1} (\sigma_{b/AP} / \sigma_{b/ML}), \quad (2)$$

where $\alpha_{b/net}$ is the angular deviation of peak stress from the ML axis. This peak stress axis is perpendicular to the net neutral axis of bending. Net longitudinal stresses at the points of peak tensile and compressive bending were then calculated as the sum of axial and bending stresses. Torsional stress (τ) due to the GRF was calculated as:

$$\tau = T (y_l / J), \quad (3)$$

where T is the torsional moment applied to the bone by the GRF (determined from the magnitude of the net GRF and its moment arm to the long axis of the femur), y_l is the distance from the centroid of the bone to its cortex, and J is the polar moment of area (Wainwright et al., 1976). For each animal, y_l was calculated as the mean of the y values from the perpendicular AP and ML directions (Table 2).

Mechanical property tests and safety factor calculations

Because published data on the bending strength of opossum femora were available for the closely related species *Didelphis marsupialis* (Erickson et al., 2002), we focused our new measurements on the mechanical properties of opossum femora in torsion (Butcher et al., 2011). Shear stresses at failure were evaluated in torsion (model 8874 biaxial testing machine with 25 kN load cell; Instron, Norwood, MA, USA) for whole bone specimens ($N=7$ femora) from our

experimental animals, as well as additional individuals used in complementary measurements of femoral strains (Butcher et al., 2011). Procedures closely followed those we have described previously in other studies (Butcher and Blob, 2008; Wilson et al., 2009; Butcher et al., 2011). Briefly, rosette strain gauges were glued to the anterior and posterior surfaces of cleaned femora for which each end was embedded ~15 mm in dental cement. Amplified strain signals were collected while bones were twisted to failure at 3 deg s⁻¹ (Furman and Saha, 2000), with tests performed to simulate *in vivo* medial (i.e. inward) rotation. Yield point was identified from plots of applied twisting moment *versus* maximum shear strain as the first point where measured strain magnitude deviated from the magnitude expected based on the initial, linear slope of the curve by 200 microstrain ($\mu\epsilon = \text{strain} \times 10^{-6}$) (Currey, 1990). Yield stresses in torsion (shear stress) were calculated from Eqn 3, using the value of T at the time of yield.

Femoral safety factors in bending were calculated as bending strength divided by peak tensile stress using the peak tensile stresses calculated from our bone stress analyses and bending strength values published for *D. marsupialis* (Erickson et al., 2002). 'Worst-case' safety factors in bending (Blob and Biewener, 2001) were also calculated as: (bending strength - 2 × standard deviation)/(peak tensile stress + 2 × standard deviation). Finally, torsional yield stresses were also compared with the shear stresses on the femur induced by the GRF, but these must be regarded cautiously in the context of safety factors because these estimates of locomotor shear stress do not account for contributions of muscle forces (see above).

Table 3. Mean peak ground reaction force (GRF) data for *D. virginiana*

Individual	Vertical GRF (BW)	AP GRF (BW)	ML GRF (BW)	Peak net GRF time (%)	Net GRF (BW)	GRF femur angle (deg)	GRF AP angle (deg)	GRF ML angle (deg)	Running speed (m s ⁻¹)
op04 (N=20)	0.56±0.02	-0.07±0.03	-0.08±0.01	33.0±1.1	0.58±0.01	16.87±1.3	-7.93±2.9	-8.0±1.2	1.35±0.04
op05 (N=13)	1.03±0.05	0.06±0.03	-0.14±0.01	30.2±1.4	1.05±0.05	14.73±1.0	2.77±1.5	-8.3±0.9	1.80±0.12
op06 (N=15)	0.74±0.04	0.11±0.02	-0.07±0.01	32.4±3.4	0.76±0.05	14.63±1.9	8.06±1.3	-6.2±1.3	1.28±0.09
op07 (N=8)	0.62±0.04	0.01±0.04	-0.05±0.02	23.3±5.7	0.63±0.05	23.68±2.8	0.93±3.2	-4.1±1.8	0.77±0.12
Mean	0.74±0.04	0.03±0.03	-0.09±0.01	29.7±2.9	0.76±0.04	17.48±1.7	0.95±2.2	-6.7±0.3	1.36±0.07

Values are means ± s.e.m. (N=number of steps analyzed).

AP, anteroposterior; BW, body weight; ML, mediolateral.

GRF femur angle, angle of GRF to the femur; GRF AP angle, anteroposterior inclination angle of GRF; GRF ML angle, mediolateral inclination angle of GRF.

Vertical=0 deg for GRF AP and ML angles of inclination; for GRF AP, negative angles are posteriorly directed and positive angles are anteriorly directed; for GRF ML, negative angles are medially directed.

RESULTS

Overview of stance phase kinematics

Opossums use a plantigrade foot posture during running with a highly extended metatarsophalangeal (MP) angle (>150 deg) for roughly half of stance, reflecting flat placement of the hindfeet on the ground. Speeds for the steps we analyzed (mean \pm s.e.m. = 1.36 ± 0.07 m s $^{-1}$; Table 3) closely matched those recorded during high-exertion treadmill trials in our study of femoral strains in opossums (Butcher et al., 2011), indicating that comparable and likely maximal levels of locomotor performance were achieved.

At the beginning of stance phase the femur is strongly adducted (mean \pm s.e.m. = -67 ± 1 deg, where 0 deg is the horizontal plane; Figs 2, 3) and in a slightly protracted position (mean \pm s.e.m. = 12 ± 1 deg, where 0 deg is vertical). The ankle and knee joints are initially extended, but reach maximal flexion by midstance as the GRF increases. The femur undergoes a small amount of additional adduction before smoothly abducting to a peak of -56 ± 1 deg shortly before the end of stance. The femur also retracts (i.e. the hip extends) roughly 40 deg through the course of stance. After reaching maximal flexion, the knee and ankle re-extend through most of the second half of stance. Rapid MP flexion occurs during the second half of stance as the rear of the foot is lifted from the ground. During final lifting of the foot in the last 10% of stance, the MP joint rapidly extends while the knee flexes and the hip adducts in preparation for swing phase.

GRF magnitude and orientation

The GRF is oriented upwards and medially for nearly all of stance phase, and directed posteriorly for approximately the first third of stance before shifting anteriorly for the remainder of the step (Figs 3, 4). Peak magnitudes of the vertical component are roughly seven times greater than those for the ML and AP components, for which peak magnitudes are similar although they occur at different times in the step (Table 3, Fig. 4A). The mean peak net GRF of 0.76 ± 0.04 BW (mean \pm s.e.m.) occurred at $29.7 \pm 2.9\%$ of stance (Table 3), with a nearly vertical orientation (pooled mean at peak net GRF: AP angle, 1.0 ± 2.2 deg; ML angle, -6.7 ± 0.3 deg; 0 deg = vertical in both directions with positive values indicating anterior and lateral inclinations; Fig. 4B). The limited medial inclination of the GRF shifted even closer to a vertical (near 0 deg; Fig. 4B) orientation through midstance until nearly the end of the step. The combination of these GRF orientations with the position of the limb through the step produced an angle of only 10–25 deg between the GRF and the femur for almost all of stance (17.5 ± 1.7 deg at peak GRF; Table 3, Fig. 4B).

Moments of the GRF about hindlimb joints

The GRF exerts a dorsiflexor moment at the ankle for almost all of stance, until the last ~10% of the step when all but the most distal portions of the toes have been lifted from the ground (Fig. 5). The ankle moment increases early in the step and then decreases through the last 75% of stance; nonetheless, extensors (i.e. plantarflexors) of the ankle would be expected to exert force to counter this moment for nearly all of stance, with biarticular members of this group also contributing to a flexor moment at the knee.

GRF moments about the knee and hip all shift direction during the course of stance as the limb moves forward over the foot during the step. The GRF initially exerts an extensor moment at the knee, but this shifts to a flexor moment (that would sum with the moment imposed by biarticular ankle extensors) before midstance (Fig. 5). Thus, for the last 50–60% of stance, knee extensors would have to be active to counter this moment in order to maintain joint

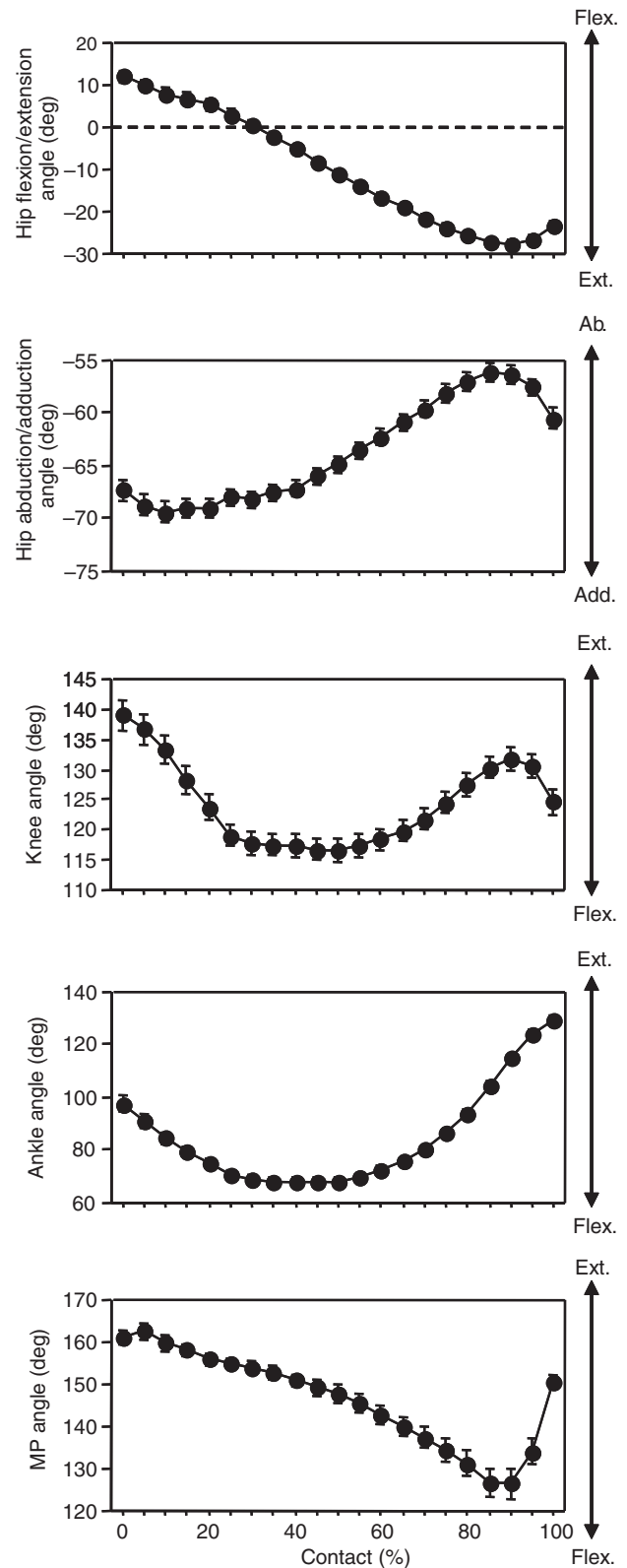


Fig. 2. Kinematic profiles of hindlimb joints for opossums (*D. virginiana*) during running steps in our force-platform experiments. Top to bottom: hip flexion (Flex.)/extension (Ext.) angle, hip abduction (Ab.)/adduction (Add.) angle, and knee, ankle and metatarsophalangeal (MP) angles. Kinematic profiles represent mean (\pm s.e.m.) angles averaged across all four opossums ($N=8-20$ trials per individual, 56 total steps per data point). Note that y-axis scales differ for these plots to provide increased resolution for smaller angles.

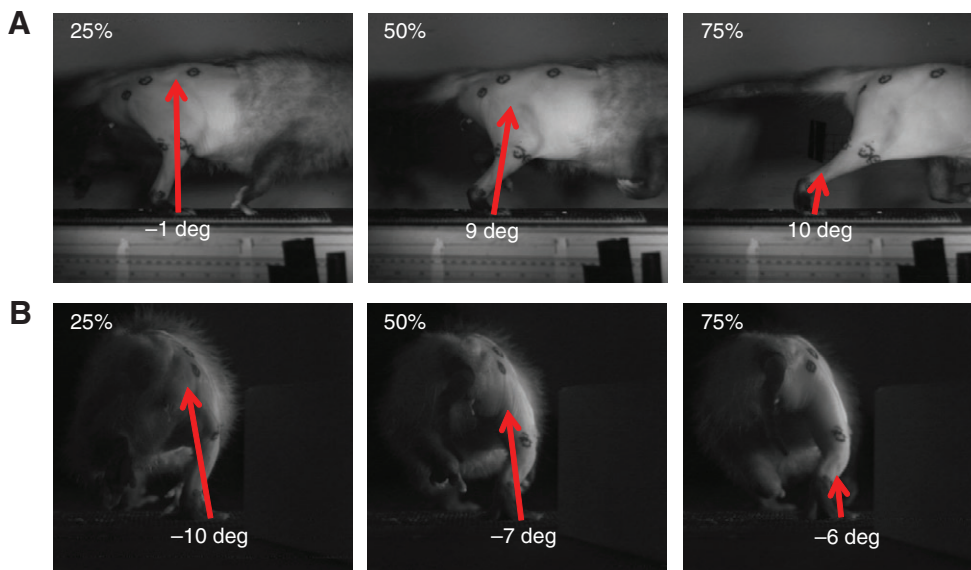


Fig. 3. Representative still images in (A) lateral and (B) posterior views from high-speed video of an opossum running over a force platform during experimental trials. Three points in time through the course of stance are indicated (percentages are labeled on each panel), and the relative magnitude and orientation of the GRF is illustrated by red arrows in each frame.

equilibrium (Fig. 6B). Very early in the step the GRF also exerts extensor and adductor moments at the hip; however, these both shift (to flexor and abductor moments, respectively) near 20% of stance (Fig. 5), indicating that activity of hip extensors and adductors would be necessary for most of the step to maintain joint equilibrium (Fig. 6B). The abductor moment appears to peak near 60% of stance (Fig. 5), just as the ML inclination of the GRF shifts to a near vertical orientation (Fig. 4).

The GRF also induces torsional moments on the femur that shift during the course of the step (Fig. 5). For the first 20% of stance (essentially matching the time during which the GRF exerts an adductor moment), these would tend to cause the right femur to rotate counterclockwise when viewed from its proximal end (i.e. inward rotation). Thereafter, the GRF would tend to rotate the right femur clockwise when viewed from its proximal end (i.e. outward rotation), reaching a peak moment at near 60% of stance.

Femoral stresses

Transverse components of the GRF impose substantial bending stresses in opossum femora in both the AP and ML directions, and the axial component of the GRF also imposes significant ML bending stress due to bone curvature (i.e. the medial offset of the femoral head to the shaft) (Fig. 6A). Stresses due to these external forces are the greatest early in stance (10–40%), when the net GRF is at its highest magnitude (Table 3). At their peaks, these forces tend to place the lateral surface of the femur in tension and the anterior surface in compression (Fig. 7). However, the limb muscles make the greatest contribution to femoral bending stress in opossums, particularly in the ML direction (Fig. 6). These peaks occur later in the step (near 60% stance; Fig. 6A) than those induced by external forces (Fig. 4A, Fig. 6A). Contraction of knee extensor muscles in opposition to the combined knee flexor moments of the GRF and biarticular ankle extensors places the anterior surface of the femur in compression, though this loading is moderated by the near simultaneous force exerted by hip extensors on the posterior aspect of the femur (Fig. 6B). Contraction of hip adductors (Fig. 6B) places the medial surface of the femur in compression and produces complementary tension on the lateral surface (Fig. 6A, Fig. 7). Peak stresses across the muscle groups we evaluated ranged roughly between 50 and 110 kPa (Fig. 6B), lower than the maximum

isometric stresses reported from limb muscles of other mammals (Wells, 1965; Alexander, 2003).

The opossum femur is loaded in axial compression and torsion as well as bending. Maximum tensile, compressive and shear stresses occurred nearly simultaneously in each step, averaging between 55 and 60% stance across all trials (Table 4, Fig. 7). This is considerably later than peak net GRF (near 30% stance; Table 3), though GRF magnitudes have typically not shown major declines by this point in the step (Fig. 4A), and hip abductor moments (Fig. 5) that might lead to elevated hip adductor forces and imposed stresses (Fig. 6) are at their maximum as the medial inclination of the GRF becomes nearly vertical (Figs 3, 4). At the time of peak tensile stress, the net plane of bending (i.e. angle of the neutral axis from the anatomical ML axis) tended to place the lateral cortex in tension and the medial cortex in compression (Fig. 7). This distribution of loading reflects the significant role of the adductor muscles in our model (Fig. 1).

Peak tensile and compressive stresses for opossum femora averaged 27.3 ± 1.2 and -35.5 ± 1.7 MPa, respectively, with no clear correlation with speed across the range used by the animals in our study. Peak compressive stresses exceed peak tensile stresses during stance (Table 4) because axial compression (-4.1 ± 0.4 MPa) is superimposed on bending. Peak femoral shear stresses (3.1 ± 0.2 MPa) are similar to axial compression in absolute magnitude (Table 4); moreover, as noted in the Materials and methods, these values are minimum estimates that reflect only the rotational moment exerted by the GRF, and do not account for torsion produced by limb muscles.

Femoral mechanical properties and safety factor calculations

Femoral yield for opossums in bending [mean \pm s.e.m. = 222 ± 12.3 MPa based on data from *D. marsupialis* (Erickson et al., 2002)] occurred at much higher stress magnitudes than femoral yield in torsion (mean \pm s.e.m. = 57.6 ± 5.2 MPa based on data from *D. virginiana*; Table 5). However, peak bending stress magnitudes are also likely much higher than peak shear stress magnitudes. Without accounting for torsional stresses imposed by limb muscles, the difference between bending and torsional stress is considerable (27.3 ± 1.2 versus 3.1 ± 0.2 MPa, respectively; Table 4), though our calculations of torsional loading likely underestimate the total shear stress on the femur to some degree. The differences in both loads

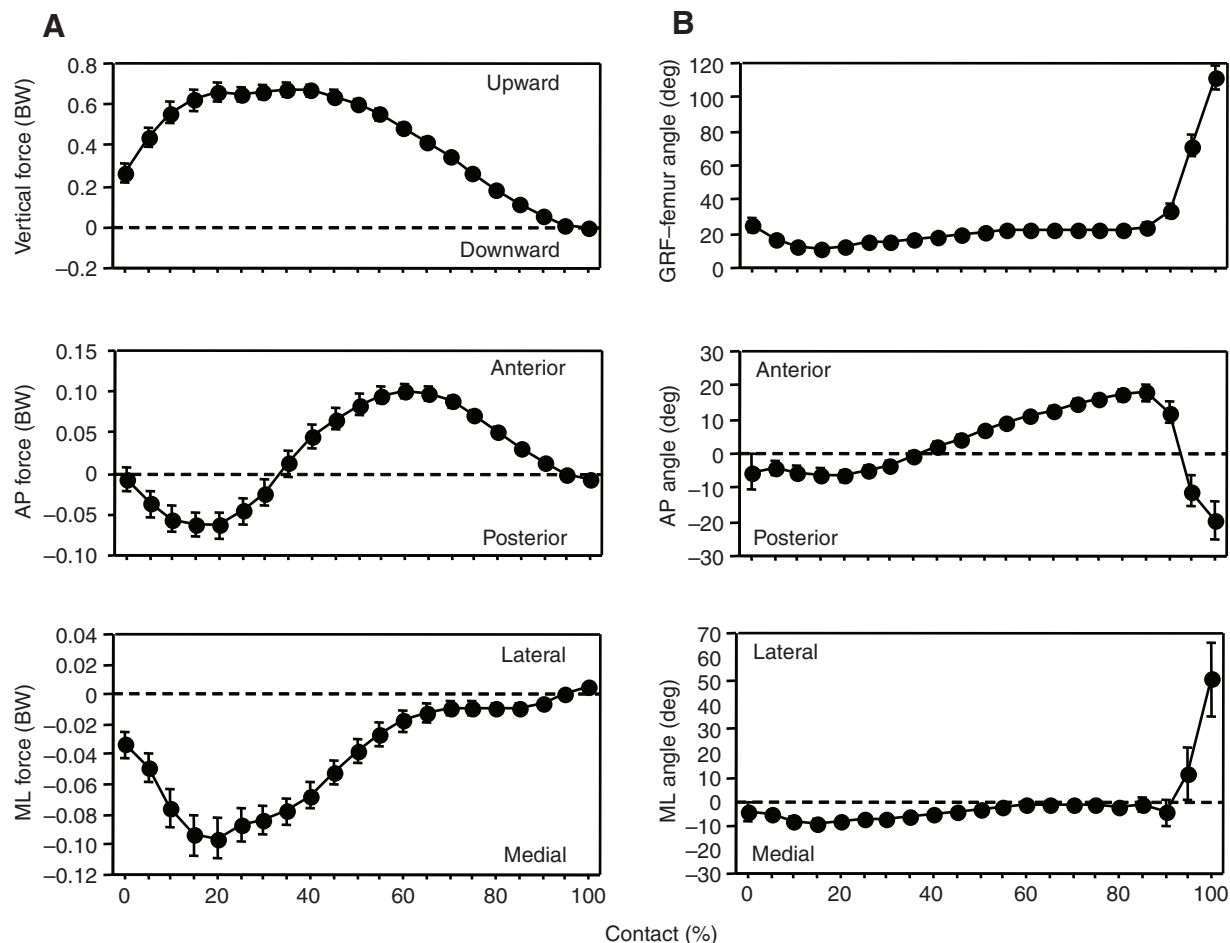


Fig. 4. Mean GRF dynamics for the right hindlimb of opossums. All plots show means (\pm s.e.m.) averaged across all four opossums ($N=8-20$ trials per individual, 56 total steps per data point). (A) Vertical, anteroposterior (AP) and mediolateral (ML) GRF components in body weight (BW), with positive values indicating upward, anterior and lateral forces, respectively (top to bottom). Y-axis scales differ for these plots to provide increased resolution for the small AP and ML forces. All trials were normalized to the same duration, allowing values to be graphed against the percentage of time through the stance. (B) Angle of the GRF (top to bottom) relative to the long axis of the femur and in the AP and ML directions. AP angles were determined relative to vertical at 0 deg (90 deg indicates horizontal GRF, pointing forward; <0 deg indicates posteriorly directed GRF). ML angles were determined relative to vertical at 0 deg (negative values indicate medially directed GRF). Femoral angles were determined relative to 0 deg at the femoral long axis.

and mechanical properties of opossum femora between bending and torsion generate estimates of safety factors for these regimes of 8.1 *versus* 18.6 (Table 5), with the more reliable estimate for bending falling within the range of 5–10 typically reported for non-avian reptiles in previous studies. ‘Worst-case’ estimates of safety factor are 6.6 for bending and 13.5 for torsion, again reflecting the likelihood that the demands that running opossums place on their limb bones, even though they are using a posture that is closer to parasagittal, result in a margin of failure similar to that seen in non-mammalian species and higher than other mammals that use a less crouched limb posture.

DISCUSSION

Loading regimes in opossum femora: the significance of torsion and ML bending

The opossum femur is loaded in a combination of axial compression, bending and torsion. Although axial compression and bending were expected based on previous studies of limb bone loading in mammals (Biewener, 1983; Biewener et al., 1983; Biewener et al., 1988), the significance of torsion was more surprising. Correlated with the use of upright limb posture and parasagittal kinematics,

particularly among larger species (e.g. dogs and horses), most previous studies of mammalian limb bone loading had found (or assumed) negligible torsion in hindlimb bones during locomotion (e.g. Alexander, 1974; Rubin and Lanyon, 1982; Biewener, 1983; Biewener et al., 1983; Biewener et al., 1988). However, the mean magnitude of shear stress induced by the GRF in opossum femora (3.1 ± 0.2 MPa) is similar in magnitude to that measured from many reptilian and amphibian species [1.0–5.8 MPa across salamanders, lizards and crocodilians (Blob and Biewener, 2001; Sheffield and Blob, 2011; Sheffield et al., 2011)]. These results corroborate findings of appreciable shear strains in opossum femora (Butcher et al., 2011) and are consistent with findings of moderate to substantial torsional loading in the femora of laboratory rats (Keller and Spengler, 1989) and terrestrial birds (Carrano, 1998; Main and Biewener, 2007). These species, like opossums, also use near-parasagittal limb kinematics and hold the femur in a crouched position for much of their stance. Given that GRF orientation during periods of peak loading is essentially similar across a wide range of species from amphibians to mammals, and spanning sprawling to upright posture (Jayes and Alexander, 1980; Biewener, 1983; Blob and Biewener, 2001; Butcher and Blob, 2008; Sheffield and

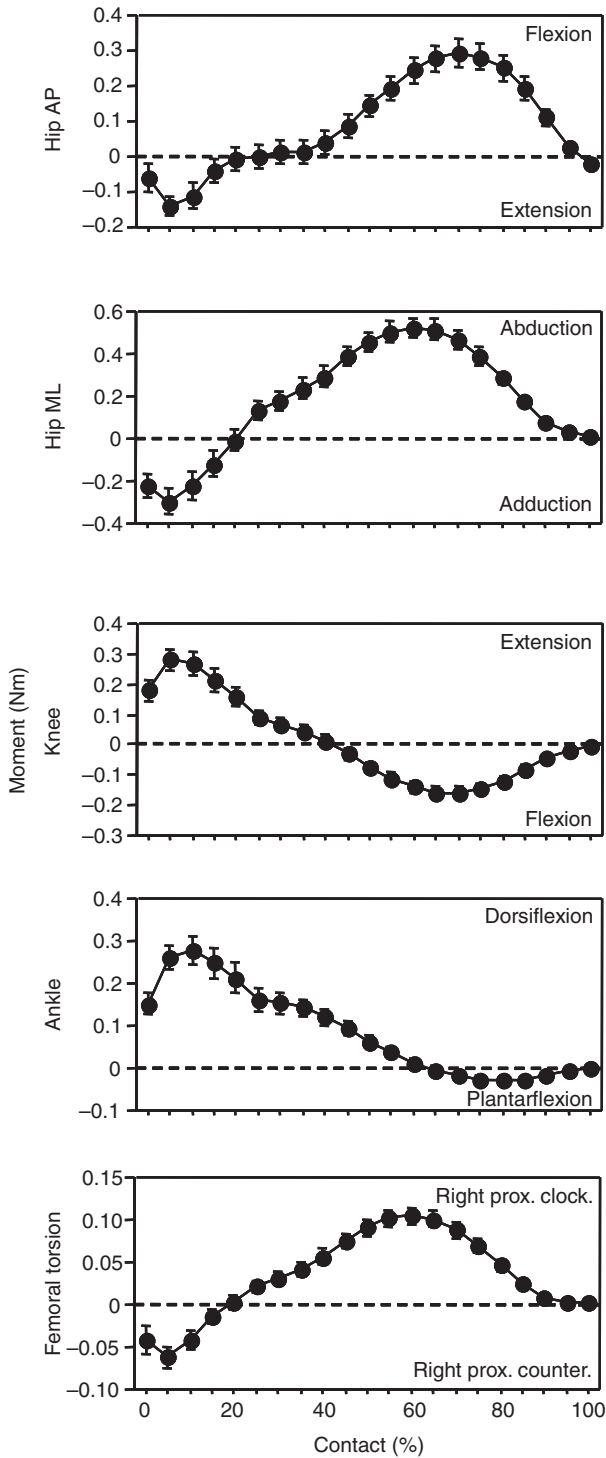


Fig. 5. Moments exerted by the GRF about the hindlimb joints and the long axis for the right femur of opossums. All plots show means (\pm s.e.m.) averaged across all four opossums ($N=8-20$ trials per individual, 56 total steps per data point). Note that y -axis scales differ for these plots to provide greater resolution for smaller moments. Directions of moments are labeled to the right of the figure plots. Hip AP, the GRF moment about the hip in the anatomical anterior and posterior directions; hip ML, the GRF moment about the hip in the anatomical medial and lateral directions; knee and ankle, the GRF moments about the knee and ankle joints; right prox. clock., torsional GRF moment, clockwise when viewing the right femur from the proximal end; right prox. counter., torsional GRF moment, counterclockwise when viewing the right femur from its proximal end.

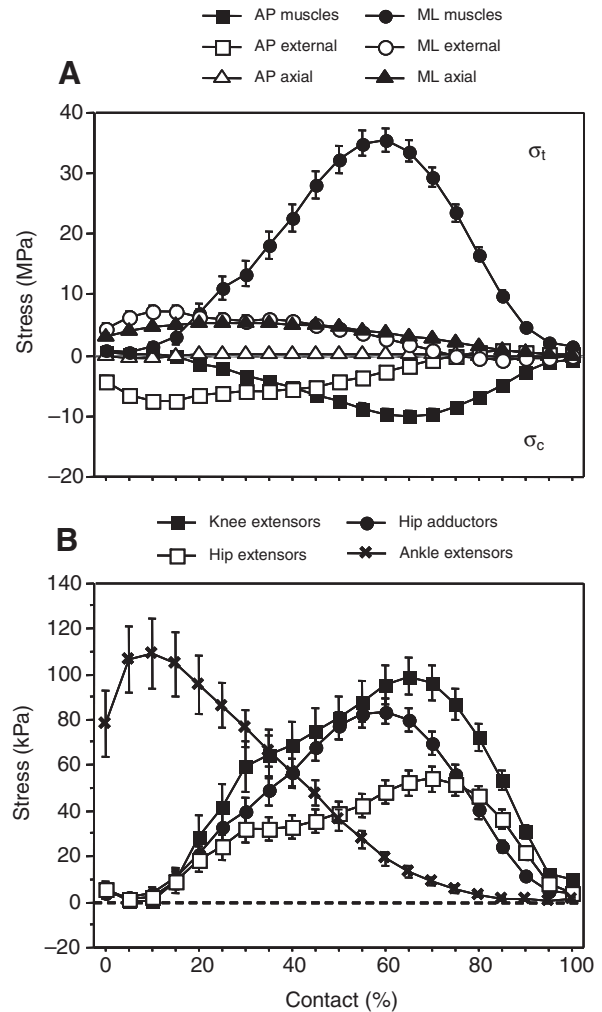
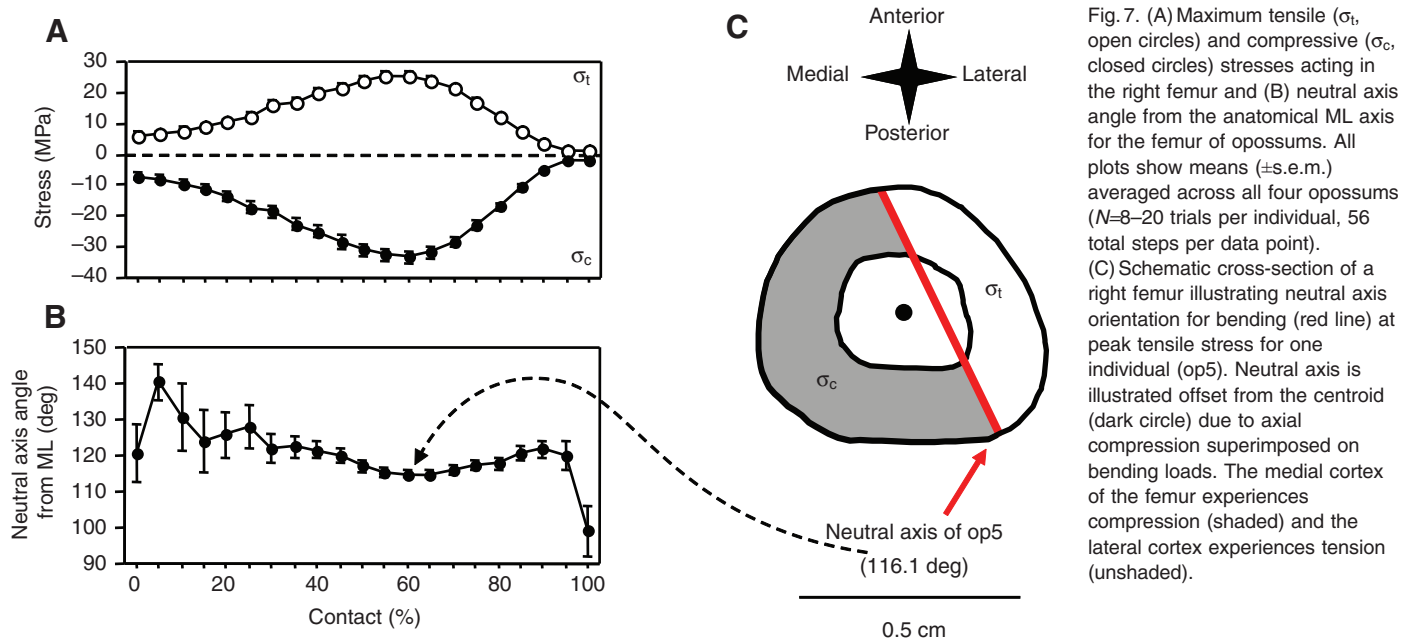


Fig. 6. (A) Components of bending stress in opossum femora induced by muscles and GRF components. Stresses plotted are those occurring on the lateral surface for forces acting to cause ML bending, and those occurring on the anterior surface for forces acting to cause AP bending. Tensile stress (σ_t) is positive and compressive stress (σ_c) is negative. 'Muscles' indicates stresses induced by major muscle groups in the direction indicated; 'external' indicates stresses induced by the GRF acting in the direction indicated; 'axial' indicates stresses induced by the axial component of the GRF due to bone curvature in the direction indicated. Bending stresses induced by axial forces are relatively small and overlap along the zero line for the AP direction. (B) Stresses calculated to act in hindlimb muscle groups (see Fig. 1) of opossums during terrestrial locomotion, based on anatomical data from Table 1. Note that the hip and knee extensors both impose AP bending but act on opposite sides of the femur, so that the net sum of femoral stress imposed by AP muscles that is plotted in A is lower in absolute magnitude than the net stress imposed by the hip adductors, plotted as ML muscles in A. This contributes to the predominance of ML femoral bending (Fig. 7). All plots in A and B show means (\pm s.e.m.) averaged across all four opossums ($N=8-20$ trials per individual, 56 total steps per data point).

Blob, 2011; Sheffield et al., 2011), these data indicate that differences in loading regimes across taxa are primarily influenced by their different limb postures. They also suggest that torsional loading may be a persistent, ancestral feature of tetrapod limb mechanics until fully upright posture is adopted.

Although bending was expected for opossum femora, the direction of bending that was identified was unexpected based on



their parasagittal limb kinematics. Previous studies of mammalian limb bone loading (e.g. Biewener, 1983; Biewener et al., 1983) had identified primarily AP bending, although some of these studies were based on only two-dimensional force data with a limited capacity to measure bending out of this plane. In an additional corroboration of results from *in vivo* strain measurements, our force-platform data also indicated a fairly close alignment of the neutral axis of bending with the anatomical AP axis, such that the medial surface of the femur was placed in tension and the lateral surface in compression (Fig. 7C). This orientation indicates a strong divergence of the direction of femoral bending from the direction of travel; however, our model of muscular forces acting on the femur provides insight into how this pattern arises.

Our use of a three-dimensional analysis allows the action of medially situated adductor muscles to be modeled in their most appropriate anatomical plane, rather grouping these muscles with posteriorly situated hip extensors as in previous studies (e.g.

Biewener, 1983). Because the GRF exerts an abductor moment for most of the step (Fig. 5), these adductors must be active for most of stance (Fig. 6B), contracting to place the medial surface of the femur in compression. This stress increases as the GRF becomes more vertical (Figs 3, 4) and its hip abductor moment arm increases (Fig. 5) towards 60% of stance, even as GRF magnitude has begun to decrease from its peak near 30% of stance. In addition, it is not substantially countered by the action of any hip abductor muscle spanning the length of the femur that could bend the bone in the opposite direction and reduce overall stress. The medial inflection of the femoral head from the shaft also increases the potential for axial forces to impose ML bending (Fig. 6A). In contrast, for bending in the AP direction, knee extensors on the anterior surface are active later in the step (Fig. 6B) against the flexor moment of the knee (Fig. 5), but these impose stress in the opposite direction from the hip extensors (on the posterior surface of the femur) or the GRF for much of the time they are active (Fig. 6), so that net AP stress

Table 4. Mean peak stresses for femora of *D. virginiana* with GRF magnitudes and orientations at peak tensile stress

Individual	N	Peak stress						Neutral axis angle from ML (deg)	Net GRF (BW)	GRF AP angle (deg)	GRF ML angle (deg)	
		Tensile (MPa)	Compressive (MPa)	Axial (MPa)	Shear (MPa)	Peak tensile time (%)	Peak compressive time (%)					Peak shear time (%)
op04	20	21.9±1.4	-28.4±1.9	-3.2±0.4	3.3±0.4	56.3±1.2	55.5±1.2	53.4±3.8	114.9±2.1	0.47±0.01	7.89±2.8	2.25±1.4
op05	13	34.4±2.4	-44.7±2.8	-5.1±0.4	4.5±0.3	60.7±1.5	60.1±1.5	59.6±1.9	116.1±1.0	0.66±0.03	10.0±2.0	-6.33±0.7
op06	15	23.4±2.7	-30.8±3.4	-3.7±0.4	2.0±0.3	63.9±3.4	64.4±3.3	63.5±2.0	107.1±1.7	0.49±0.03	10.0±1.0	-1.38±1.2
op07	8	36.5±2.1	-47.0±3.0	-5.3±0.5	2.7±0.2	55.0±2.8	55.8±2.9	48.6±7.5	112.9±0.9	0.48±0.03	4.38±1.2	-1.02±1.1
Mean	56	27.3±1.2	-35.5±1.7	-4.1±0.4	3.1±0.2	59.0±2.2	59.1±2.2	56.3±3.8	112.7±1.4	0.52±0.03	8.07±1.7	-1.62±1.1

Values are means ± s.e.m. (N=number of steps analyzed).

Axial stresses are reported at the time of peak tensile stress.

Shear stresses are reported for counterclockwise rotations of the right femur as viewed from the proximal end.

Peak tension and compression times are shown as a percentage of stance.

Deviations of the neutral axis from the anatomical mediolateral (ML) axis of each bone are counterclockwise in direction (i.e. positive angle from horizontal at 0 deg).

AP, anteroposterior.

Vertical=0 deg for GRF AP and ML angles of inclination; for GRF AP, positive angles are anteriorly directed; for GRF ML, negative angles are medially directed and positive angles are laterally directed.

Table 5. Mechanical properties and safety factors for opossum femora

Bending			Shear		
Yield stress (MPa)	Peak stress (MPa)	Safety factor	Yield stress (MPa)	Peak stress (MPa)	Safety factor
222±12.3*	27.3±1.2	8.1	57.6±5.2	3.1±0.2	18.6

Values are means ± s.e.m.

Peak shear stress calculations account only for stresses imposed by the GRF, and do not account for shear stress imposed by muscles.

*Value for *Didelphis marsupialis* (Erickson et al., 2002).

is minimized. This combination of strong adductor muscle activity and minimization of bending imposed by anteriorly and posteriorly situated muscles generates a predominantly ML pattern of bending (Fig. 7) despite the main AP oscillation of the limbs during running.

Safety factors in opossum femora: mechanical basis and evolutionary implications

Safety factors of the opossum femora were determined to be 8.1 in bending and potentially as high as 18.6 in torsion, though (as noted previously) this latter value does not account for torsional stresses induced by limb muscles. This value for bending is relatively similar to strain-based estimates of femoral safety factors for opossums, which range between 5 and 8 (Butcher et al., 2011). Though there are differences in safety factor estimates between the two experimental approaches, the presence of such differences has been noted in other comparisons of these techniques (Biewener et al., 1983; Butcher et al., 2008).

Like the corresponding strain data, the opossum safety factors obtained through this stress analysis were moderately higher than the safety factors of other mammals and at least as high as the safety factors calculated for reptiles and amphibians in recent studies (Blob and Biewener, 2001; Butcher and Blob, 2008; Sheffield and Blob, 2011; Sheffield et al., 2011). The mechanical properties of opossum limb bones are not especially distinctive compared with those of other taxa (Currey, 1987; Erickson et al., 2002; Wilson et al., 2009). Instead, opossum safety factors are higher than those of most mammals because the magnitudes of loads they experience are lower (by a factor of two or more for some species; Table 4). Although the running speeds we measured (Table 3) indicated that our opossums were approaching their maximal performance (Butcher et al., 2011), muscle stresses were moderate (Fig. 6B) and it is possible that limb bone loads might be higher (and safety factors lower) in opossums if they simply performed more taxing locomotor behaviors. For example, unlike many mammalian species in which limb bone safety factors have been measured [e.g. horses (Biewener et al., 1983; Biewener et al., 1988)], opossums are constrained to trotting, rather than transitioning to a gallop, as they run at higher speeds (Peters et al., 1984; White, 1990; Reilly and White, 2003). Yet, the question remains why high limb bone safety factors might be maintained in opossums despite the potentially lower demands that they face (Sheffield et al., 2011). One possibility is that such safety factors are simply not sufficiently disadvantageous to be selected against (Blob and Biewener, 1999; Sheffield et al., 2011).

A further outstanding question is the nature of the evolutionary association between limb posture and limb bone loading magnitudes. Did upright posture help to keep increasing limb bone loads in check, or might elevated loads actually have accompanied the evolution of more upright posture? Historical data to evaluate these alternatives would be challenging to gather. However, the recognition that, within animals that use a range of limb postures, loads often increase with the use of more upright stance (Blob and Biewener, 1999; Blob and Biewener, 2001; Reilly and Blob, 2003) suggests that the

evolution of upright posture in mammals may have carried accommodation of higher limb bone loading as a consequence (Blob, 2001).

ACKNOWLEDGEMENTS

We thank J. Parrish, T. Pruitt, T. Smith, T. Parker and D. Bailey for assistance with animal care at the Godley-Snell Research Center (Clemson); A. Rivera for improving MATLAB analysis code; and T. Higham, J. DesJardins, E. Alvarez and two anonymous reviewers for comments on the manuscript. J. DesJardins, E. Alvarez and R. Rusly provided access to and assistance with mechanical testing equipment; C. Templeton and J. Scott (Clemson) assisted with mechanical property analyses; and S. Bennett (South Carolina Department of Natural Resources) coordinated permission for field collection of opossums (SCDNR Scientific Collecting Permits 54-2008 and 40-2009). Additional assistance with opossum collection was provided by J. Gosnell, J. Cummings, H. Schoenfuss, L. Schoenfuss, and the Animal Control Departments of Pickens County and Pendleton, SC. Portions of this work were submitted as an MSc Thesis at Clemson University by W.C.G. Support by NSF (IOB-0517340) and the Clemson University and Youngstown State University Departments of Biological Sciences are gratefully acknowledged.

REFERENCES

- Alexander, R. M. (1974). The mechanics of a dog jumping, *Canis familiaris*. *J. Zool. Lond.* **173**, 549-573.
- Alexander, R. M. (2003). *Principles of Animal Locomotion*. Princeton, NJ: Princeton University Press.
- Beer, F. P. and Johnston, E. R., Jr (1997). *Vector Mechanics for Engineers: Statics and Dynamics*, 6th edn. Boston, MA: McGraw-Hill.
- Biewener, A. A. (1983). Locomotor stresses in the limb bones of two small mammals: the ground squirrel and chipmunk. *J. Exp. Biol.* **103**, 131-154.
- Biewener, A. A. (1990). Biomechanics of mammalian terrestrial locomotion. *Science* **250**, 1097-1103.
- Biewener, A. A. (1993). Safety factors in bone strength. *Calcif. Tissue Int.* **53 Suppl.** **1**, S68-S74.
- Biewener, A. A. and Full, R. J. (1992). Force platform and kinematic analysis. In *Biomechanics – Structures and Systems: A Practical Approach* (ed. A. A. Biewener), pp. 45-73. New York: Oxford University Press.
- Biewener, A. A. and Taylor, C. R. (1986). Bone strain: a determinant of gait and speed? *J. Exp. Biol.* **123**, 383-400.
- Biewener, A. A., Thomason, J., Goodship, A. and Lanyon, L. E. (1983). Bone stress in the horse forelimb during locomotion at different gaits: a comparison of two experimental methods. *J. Biomech.* **16**, 565-576.
- Biewener, A. A., Thomason, J. and Lanyon, L. E. (1988). Mechanics of locomotion and jumping in the horse (*Equus*): *in vivo* stress in the tibia and metatarsus. *J. Zool. Lond.* **214**, 547-565.
- Blob, R. W. (2001). Evolution of hindlimb posture in non-mammalian therapsids: biomechanical tests of paleontological hypotheses. *Paleobiology* **27**, 14-38.
- Blob, R. W. and Biewener, A. A. (1999). *In vivo* locomotor strain in the hindlimb bones of *Alligator mississippiensis* and *Iguana iguana*: implications for the evolution of limb bone safety factor and non-sprawling limb posture. *J. Exp. Biol.* **202**, 1023-1046.
- Blob, R. W. and Biewener, A. A. (2001). Mechanics of limb bone loading during terrestrial locomotion in the green iguana (*Iguana iguana*) and American alligator (*Alligator mississippiensis*). *J. Exp. Biol.* **204**, 1099-1122.
- Butcher, M. T. and Blob, R. W. (2008). Mechanics of limb bone loading during terrestrial locomotion in river cooter turtles (*Pseudemys concinna*). *J. Exp. Biol.* **211**, 1187-1202.
- Butcher, M. T., Espinoza, N. R., Cirilo, S. R. and Blob, R. W. (2008). *In vivo* strains in the femur of river cooter turtles (*Pseudemys concinna*) during terrestrial locomotion: tests of force-platform models of loading mechanics. *J. Exp. Biol.* **211**, 2397-2407.
- Butcher, M. T., White, B. J., Hudzik, N. B., Gosnell, W. C., Parrish, J. H. A. and Blob, R. W. (2011). *In vivo* strains in the femur of the Virginia opossum (*Didelphis virginiana*) during terrestrial locomotion: testing hypotheses of evolutionary shifts in mammalian bone loading and design. *J. Exp. Biol.* **214**, 2631-2640.
- Carrano, M. T. (1998). Locomotion of non-avian dinosaurs: integrating data from hindlimb kinematics, *in vivo* strains and bone morphology. *Paleobiology* **24**, 450-469.
- Carrier, D. R., Heglund, N. C. and Earls, K. D. (1994). Variable gearing during locomotion in the human musculoskeletal system. *Science* **265**, 651-653.
- Currey, J. D. (1987). The evolution of the mechanical properties of amniote bone. *J. Biomech.* **20**, 1035-1044.

- Currey, J. D.** (1990). Physical characteristics affecting the tensile failure properties of compact bone. *J. Biomech.* **23**, 837-844.
- Erickson, G. M., Catanese, J., 3rd and Keaveny, T. M.** (2002). Evolution of the biomechanical material properties of the femur. *Anat. Rec.* **268**, 115-124.
- Furman, B. R. and Saha, S.** (2000). Torsional testing of bone. In *Mechanical Testing of Bone and the Bone-Implant Interface* (ed. Y. H. An and R. A. Draughn), pp. 219-239. Boca Raton, FL: CRC Press.
- Gillis, G. B. and Biewener, A. A.** (2001). Hindlimb muscle function in relation to speed and gait: *in vivo* patterns of strain and activation in a hip and knee extensor of the rat (*Rattus norvegicus*). *J. Exp. Biol.* **204**, 2717-2731.
- Gruner, J. A. and Altman, J.** (1980). Swimming in the rat – analysis of locomotor performance in comparison to stepping. *Exp. Brain Res.* **40**, 374-382.
- Hedrick, T. L.** (2008). Software techniques for two- and three-dimensional kinematic measurements of biological and biomimetic systems. *Bioinspir. Biomim.* **3**, 034001.
- Jayes, A. S. and Alexander, R. McN.** (1980). The gaits of chelonians: walking techniques for very slow speeds. *J. Zool. Lond.* **191**, 353-378.
- Jenkins, F. A., Jr** (1971). Limb posture and locomotion in the Virginia opossum (*Didelphis marsupialis*) and in other cursorial mammals. *J. Zool. Lond.* **165**, 303-315.
- Keller, T. S. and Spengler, D. M.** (1989). Regulation of bone stress and strain in the immature and mature rat femur. *J. Biomech.* **22**, 1115-1127.
- Kemp, T. S.** (1982). *Mammal-like Reptiles and the Origin of Mammals*. London: Academic Press.
- Lieberman, D. E., Pearson, O. M., Polk, J. D., Demes, B. and Crompton, A. W.** (2003). Optimization of bone growth and remodeling in response to loading in tapered mammalian limbs. *J. Exp. Biol.* **206**, 3125-3138.
- Main, R. P. and Biewener, A. A.** (2007). Skeletal strain patterns and growth in the emu hindlimb during ontogeny. *J. Exp. Biol.* **210**, 2676-2690.
- Meyer, A. and Zardoya, R.** (2003). Recent advances in the (molecular) phylogeny of vertebrates. *Annu. Rev. Ecol. Evol. Syst.* **34**, 311-338.
- Peters, S. E., Mulkey, R., Rasmussen, S. A. and Goslow, G. E., Jr** (1984). Motor units of the primary ankle muscles of the opossum (*Didelphis virginiana*): functional properties and fiber types. *J. Morphol.* **181**, 305-317.
- Rasmussen, S., Chan, A. K. and Goslow, G. E.** (1978). The cat step cycle: electromyographic patterns for hindlimb muscles during posture and unrestrained locomotion. *J. Morphol.* **155**, 253-269.
- Reilly, S. M. and Blob, R. W.** (2003). Motor control of locomotor hindlimb posture in the American alligator (*Alligator mississippiensis*). *J. Exp. Biol.* **203**, 4327-4340.
- Reilly, S. M. and White, T. D.** (2003). Hypaxial motor patterns and the function of epipubic bones in primitive mammals. *Science* **299**, 400-402.
- Romer, A. S.** (1922). The locomotor apparatus of certain primitive and mammal-like reptiles. *Bull. Am. Mus. Nat. Hist.* **46**, 517-606.
- Roy, R. R., Hutchison, D. L., Pierotti, D. J., Hodgson, J. A. and Edgerton, V. R.** (1991). EMG patterns of rat ankle extensors and flexors during treadmill locomotion and swimming. *J. Appl. Physiol.* **70**, 2522-2529.
- Rubin, C. T. and Lanyon, L. E.** (1982). Limb mechanics as a function of speed and gait: a study of functional strains in the radius and tibia of horse and dog. *J. Exp. Biol.* **101**, 187-211.
- Schoenfuss, H. L., Roos, J. D., Rivera, A. R. V. and Blob, R. W.** (2010). Motor patterns of distal hind limb muscles in walking turtles: implications for models of limb bone loading. *J. Morphol.* **271**, 1527-1536.
- Sheffield, K. M. and Blob, R. W.** (2011). Loading mechanics of the femur in tiger salamanders (*Ambystoma tigrinum*) during terrestrial locomotion. *J. Exp. Biol.* **214**, 2603-2615.
- Sheffield, K. M., Butcher, M. T., Shugart, S. K., Gander, J. C. and Blob, R. W.** (2011). Locomotor loading mechanics in the hindlimbs of tegu lizards (*Tupinambis merianae*): comparative and evolutionary implications. *J. Exp. Biol.* **214**, 2616-2630.
- Sullivan, T. E. and Armstrong, R. B.** (1978). Rat locomotory muscle-fiber activity during trotting and galloping. *J. Appl. Physiol.* **44**, 358-363.
- Thota, A. K., Watson, S. C., Knapp, E., Thompson, B. and Jung, R.** (2005). Neurochemical control of locomotion in the rat. *J. Neurotrauma* **22**, 442-465.
- Wainwright, S. A., Biggs, W. D., Currey, J. D. and Gosline, J. M.** (1976). *Mechanical Design in Organisms*. Princeton: Princeton University Press.
- Walker, J. A.** (1998). Estimating velocities and accelerations of animal locomotion: a simulation experiment comparing numerical differentiation algorithms. *J. Exp. Biol.* **201**, 981-995.
- Wells, J. B.** (1965). Comparison of mechanical properties between slow and fast mammalian muscles. *J. Physiol.* **178**, 252-269.
- White, T. D.** (1990). Gait selection in the brush-tail possum (*Trichosurus vulpecula*), the northern quoll (*Dasyurus hallucatus*), and the Virginia opossum (*Didelphis virginiana*). *J. Mammal.* **71**, 79-84.
- Wilson, M. P., Espinoza, N. R., Shah, S. R. and Blob, R. W.** (2009). Mechanical properties of the hindlimb bones of bullfrogs and cane toads in bending and torsion. *Anat. Rec.* **292**, 935-944.